

# Characterizing the automatic radon flux Transfer Standard system *Autoflux*: laboratory calibration and field experiments

Claudia Grossi<sup>1,2</sup>, Daniel Rabago<sup>3</sup>, Scott Chambers<sup>4</sup>, Carlos Sáinz<sup>3</sup>, Roger Curcoll<sup>1</sup>, Peter PS. Otáhal<sup>5</sup>, Eliška Fialová<sup>5,6</sup>, Luis Quindos<sup>3</sup>, Arturo Vargas<sup>1</sup>

<sup>1</sup> Institut de Tècniques Energètiques, Universitat Politècnica de Catalunya, 08028 Barcelona, Spain

<sup>2</sup> Physics Department, Universitat Politècnica de Catalunya, 08028 Barcelona, Spain

<sup>3</sup> Universidad de Cantabria, 39011 Santander, Spain

<sup>4</sup> ANSTO, Environmental Research, Lucas Heights, NSW 2234, Australia

<sup>5</sup> Nuclear Protection Department, National Institute for Nuclear, Chemical & Biological Protection, Milin 26231, Czech Republic

<sup>6</sup> Department of Geological Sciences, Faculty of Science, Masaryk University, 60200 Brno, Czech Republic

Correspondence to: Claudia Grossi (claudia.grossi@upc.edu)

## Abstract

High-quality, long-term measurements of terrestrial trace gas emissions are important for investigations of atmospheric, geophysical and biological processes to help mitigate climate change, protect the environment, and the health of citizens. High-frequency terrestrial fluxes of the radioactive noble gas  $^{222}\text{Rn}$ , in particular, are useful for validating radon flux maps, used to evaluate the performance of regional atmospheric models, to improve greenhouse gas emission inventories (by the Radon Tracer Method) and to determine Radon Priority Areas for radiation protection goals.

A new automatic radon flux system (the *Autoflux*) was developed as a Transfer Standard (TS) to assist with establishing a traceability chain for field-based radon flux measurements. The operational characteristics and features of the system were optimized based on a literature review of existing flux measurement systems. To characterize and calibrate the *Autoflux* a bespoke radon Exhalation Bed (EB) facility was also constructed with the intended purpose of providing a constant radon exhalation under a specific set of controlled laboratory conditions. The calibrated *Autoflux* was then used to transfer the derived calibration to a second continuous radon flux system under laboratory conditions, both instruments were then tested in the field and compared with modeled fluxes.

This paper presents: i) a literature review of state-of-the-art radon flux systems and EB facilities; ii) the design, characterization and calibration of a reference radon EB facility; iii) the design, characterization and calibration of the *Autoflux* system; iv) the calibration of a second radon flux system (*INTE\_Flux*) using the EB and *Autoflux*, with a total uncertainty of 9% ( $k=1$ ) for an average radon flux of  $\sim 1800 \text{ mBq m}^{-2} \text{ s}^{-1}$  under controlled laboratory conditions; and v) an example application of the calibrated TS and *INTE\_Flux* systems for in situ radon flux measurements which are then compared with simulated radon fluxes. Calibration of the TS under different environmental conditions and at lower reference fluxes will be the subject of a separate future investigation.

## 1 Introduction

The radioactive, noble gas radon ( $^{222}\text{Rn}$ ) contributes over half of the total public radiation dose from natural sources (WHO, 2009). However, due to its short half-life (3.8 days) and chemical inertness, radon is also widely used as an environmental tracer for atmospheric and geophysical processes (Grossi et al., 2012; Vargas et al., 2015; Chambers et al., 2016; Chambers et al., 2018; Zhang et al., 2021). In particular, climate scientists are using co-located measurements of atmospheric radon and greenhouse gas (GHG) concentrations to apply the so-called Radon Tracer Method (RTM) for estimating local- to regional-scale GHG emissions (Grossi et al., 2018; Levin et al., 2021).

These applications require information, at high temporal resolution and low uncertainty, about: i) the quantity of radon emitted per unit area and time from a surface of interest (the radon flux,  $F$ , or exhalation rate; usually expressed in  $\text{mBq m}^{-2} \text{ s}^{-1}$ ); and ii) the atmospheric radon activity concentration (SI units  $\text{Bq m}^{-3}$ ).

Terrestrial radon exhalation is the result of  $^{222}\text{Rn}$  escape from soil pore spaces to the atmosphere after its formation by  $^{226}\text{Ra}$  decay (Nazaroff, 1992).  $^{222}\text{Rn}$  exhalation rates are primarily driven by diffusion processes and depend strongly on the soil  $^{226}\text{Ra}$  content and soil properties (porosity, tortuosity, soil humidity, etc.). Consequently, the  $^{238}\text{U}$  content and parameters influencing diffusive transport in the soil need to be known to properly estimate the

56 spatial and temporal variability of  $^{222}\text{Rn}$  exhalation rates (Schübler, 1996; Lopez-Coto et al., 2013; Karstens et al.,  
57 2015). Furthermore, the emanation factor of radon from the soil grains to the pore spaces is influenced by soil  
58 humidity (Nazaroff, 1992; Zhuo et al., 2006; Zhuo et al., 2008).

59 Although diffusion is the primary transport mechanism of radon in soils, driven by the strong vertical concentration  
60 gradient (Karstens et al., 2015), advective transport can also occur, but this has not been thoroughly investigated  
61 and is likely to be highly site specific. Advective transport typically results from local pressure gradients, changing  
62 wind speed and direction, etc. Consequently, advective processes could influence radon flux measurements  
63 (Gutiérrez-Álvarez et al. 2020a). Other factors including soil type, atmospheric pressure, rainfall (related to soil  
64 moisture), and soil temperature can affect the radon flux. However, complex dependencies between these factors  
65 makes it difficult to quantify changes in radon flux due to any one of these factors in isolation (e.g., a precipitation  
66 event is often also associated with a drop in pressure and temperature).

67 To date, most radon flux studies have been based on random sampling and short temporal measurement data, due  
68 to the lack of robust continuous radon flux systems. Unfortunately, these kinds of datasets are not sufficient to  
69 clarify relationships between radon flux and environmental factors. This is also a contributing factor to why some  
70 studies reach contradictory conclusions about the influence of individual parameters on the radon flux.

71 Long-term, reliable radon flux measurements are needed in conjunction with corresponding environmental  
72 observations in the soil and lower atmosphere (McLaughlin, 2011; Yang et al., 2017). To ensure reliable  
73 measurements it is important to characterize and calibrate the operational radon flux systems, which requires: i) a  
74  $^{222}\text{Rn}$  Exhalation Bed (EB) facility, to provide reference radon fluxes under controlled laboratory conditions; ii) a  
75 Transfer Standard (TS) instrument to be calibrated using the EB and used as a reference monitor for calibrating  
76 other new or existing monitors, or to be used directly for in situ measurement campaigns; and iii) planned field-  
77 based inter-comparison campaigns of different radon flux systems under in situ environmental conditions.

78 The need of an EB facility is justified because, despite the fact that the response of the radon monitors itself can  
79 be previously studied within a STAR (System for Test Atmospheres with Radon) by comparison with a known  
80 reference radon concentration, and that geometries of external volumes making the radon flux systems could be  
81 measured separately with their own uncertainties, the total tubes and internal volumes estimation could lead to  
82 high uncertainties. Thus, comparing the radon flux systems response with reference exhalation bed will allow to  
83 characterize the effective height of the systems, needed for the flux calculation, with the minimum uncertainty.

84 One of the main aims of the EMPIR 19ENV01 project (henceforth traceRadon), which started in June 2020, was  
85 to provide the necessary measurement infrastructure and transfer standards to enable traceable radon flux and  
86 atmospheric radon activity concentration measurements. These goals are being achieved in collaboration with,  
87 among other research groups, the Integrated Carbon Observation System (ICOS, [www.icos-cp.eu](http://www.icos-cp.eu)) network, whose  
88 researchers are interested in introducing traceable radon flux and atmospheric radon concentration measurements  
89 to sites within this network for RTM applications.

90 The specific contributions of this study to the overall traceRadon objectives are to offer a calibrated and  
91 characterized continuous TS system, equipped with soil and atmosphere sensors, that can be used to carry out  
92 radon flux campaigns at different sites to help improve and evaluate the performance of contemporary radon flux  
93 maps and models (Szegvary et al., 2009; Karstens et al., 2015), as well as be used to calibrate other radon flux  
94 systems under laboratory or field conditions.

95 The remainder of this manuscript is arranged in the following way: first, a review is made of state-of-the-art EB  
96 facilities, including a description of the one newly designed, built and characterized by Cantabria University for  
97 the traceRadon project; next, a review is presented of contemporary, available state-of-the-art radon flux systems,  
98 including a description of the new automated system (*AutoFlux*) designed, characterized and calibrated by the  
99 Australian Nuclear Science and Technology Organization (ANSTO) and the Universitat Politècnica de Catalunya  
100 (UPC); next, the protocol applied to calibrate another automatic radon flux system (*INTE\_Flux*), designed by the  
101 Institute of Energy Technologies of the UPC, using the *AutoFlux* and the UC EB facility is described. Finally, both  
102 radon flux systems are tested during a field-based intercomparison campaign and the results compared with  
103 previous tests of these systems and with radon flux model outputs available at the ICOS Carbon Portal ([www.icos-  
104 cp.eu/](http://www.icos-<br/>104 cp.eu/)).

105

## 106 2 Materials and Methods

107

### 108 2.1. Overview of theoretical radon flux estimation

109

110 A review of relevant literature found that radon flux studies have historically been carried out using a theoretical  
111 value as a reference. IAEA (1992) suggested that radon flux systems should be calibrated using a thin layer model,  
112 under the assumption of ‘pure’ diffusion and a soil with well characterized  $^{226}\text{Ra}$  activity concentration, depth  
113 (thickness), porosity, and radon emanation characteristics (UNSCEAR, 1988; Rogers & Nielson, 1991; Nazaroff,  
114 1992; Porstendörfer, 1994). In contrast, most contemporary radon flux studies have been based on the experimental  
115 accumulation chamber method (Hassan et al., 2009), resulting in a standard method reflected in the ISO 11665-  
116 7:2012: *Accumulation method for estimating surface exhalation rate*. In these cases, the reference value used for  
117 calibration of the radon flux system, and method of flux measurement, is based on the results of an exponential fit  
118 of the increasing radon activity concentration inside a chamber of known volume, or in a STAR (ISO, 2009),  
119 during several days.

120 The theoretical approach enables calculation of the radon flux ( $F$ ) by the diffusion equation (Porstendörfer, 1994):

$$F = \varepsilon \cdot C_{\text{Ra}} \cdot \rho \cdot L \cdot \lambda \cdot \tanh\left(\frac{z}{L}\right) \quad (1)$$

121 where  $\varepsilon$  is the radon emanation factor,  $C_{\text{Ra}}$  is the  $^{226}\text{Ra}$  activity of the soil ( $\text{Bq kg}^{-1}$ ),  $\rho$  the dry bulk density ( $\text{kg m}^{-3}$ )  
122 of the soil,  $L$  the radon diffusion length in the soil (m),  $z$  is the soil thickness (m) and  $\lambda$  is the radon decay  
123 constant ( $2.0993 \cdot 10^{-6} \text{ s}^{-1}$  following Morawska, 1989).

124 Within Eq. 1, the emanation factor is defined to be the fraction of radon atoms produced by radium disintegration  
125 that escape into the soil pore space. Its value varies between 0, when radon does not escape the  $^{226}\text{Ra}$ -containing  
126 soil grain, and 1, when all radon escapes. This factor depends on many things, including: grain size and shape,  
127 moisture content, porosity, permeability, and the distribution of  $^{226}\text{Ra}$  atoms in the mineral grains (Baskaran, 2016).

128 Considering a soil sample of a determinate mass, where the sample is sufficiently well distributed to ensure that  
129 all radon atoms successfully entering the pore spaces of the sample will eventually escape to the air volume and  
130 be measured, the emanation factor  $\varepsilon$  can be defined as:

$$\varepsilon = \frac{A_{\text{Rn}}}{A_{\text{Ra}}} \quad (2)$$

131 where  $A_{\text{Ra}}$  is the total radium activity of the sample, and  $A_{\text{Rn}}$ , the radon activity that escapes from the sample. The  
132 radium activity is usually measured by gamma spectrometric analysis of the soil sample (i.e., Quindos et al., 1994).  
133 To determine the radon activity that escapes from the sample, an airtight stainless-steel container of known volume  
134 is commonly used, and the rate of escape is determined by the increase in radon concentration inside (i.e., Stoulos  
135 et al., 2004).

136 The bulk density,  $\rho$ , can be calculated from the sample weight and volume of the dry soil (Hosoda, 2007). When  
137 the soil thickness is much smaller than the radon diffusion length (i.e.,  $z \ll L$ ), as is the case for the Exhalation  
138 Bed used in this study, the approximation  $\tanh(z/L) \approx z/L$  can be used. Thus, the final equation will be (Lopez-  
139 Coto et al., 2009):

$$F = \varepsilon \cdot C_{\text{Ra}} \cdot \rho \cdot \lambda \cdot z \quad (3)$$

140 In order to prove the applicability of Eq. 3, the diffusion length  $L$  has to be evaluated and compared with  $z$ .  $L$  can  
141 be estimated as:

$$L = \sqrt{D/\lambda} \quad (4)$$

142 where  $D$  is the effective diffusion coefficient of the trace gas in the soil air (hereafter also named effective  
143 diffusivity).  $D$  is assumed to be constant with depth (Karstens et al., 2015), and can be estimated from water  
144 saturation  $w_s$  and porosity  $p$  using the following expression (Rogers and Nielson, 1991; Prasad et al., 2012):

$$D = D_{\text{air}} \cdot p \cdot \exp(-6w_s p - 6w_s^{14p}) \quad (5)$$

145 where  $D_{\text{air}}$  is the radon diffusion coefficient in air ( $1.1 \cdot 10^{-5} \text{ m}^2 \text{ s}^{-1}$ ).

146 Karstens et al., (2015) made reference to Jin and Jury (1996) and Millington and Quirk (1960) who proposed, and  
 147 verified, another experimental estimation of the effective diffusivity:

$$148 \quad D = D_{air} \cdot \frac{(p-w_V)^2}{p^{2/3}} \quad (5a)$$

149 where  $w_V$  ( $m^3/m^3$ ) is the Volume Water Content (VWC) of the soil. Equations 5 and 5a were both derived  
 150 empirically and are quite consistent with each other, mainly for dry soils, as will be shown in the following sections.

151 The porosity and water saturation  $w_s$  ( $m^3/m^3$ ) (Idoria et al., 2020; IAEA, 2013) are given by:

$$p = 1 - \frac{\rho}{\rho_g} \quad (6)$$

152 where  $\rho_g$  is the grain density, and:

$$w_s = \frac{\rho \cdot w_c}{p \cdot \rho_w} \quad (7)$$

153

154 where  $w_c$  (kg/kg) is the mass water content of the soil sample and  $\rho_w$  is the water density ( $1000 \text{ kg/m}^3$ ). Karstens  
 155 et al., (2015) reported that the temperature dependence of  $^{222}\text{Rn}$  diffusivity could also be estimated according to  
 156 Schery and Wasiolek (1998):

$$D(T) = D_0 \left( \frac{T}{T_0} \right)^{3/2} \quad (8)$$

157

158 where  $T$  is the mean soil temperature in Kelvin and  $D_0$  the effective diffusivity at the reference temperature  $T_0 =$   
 159  $273 \text{ K}$ .

160 The experimental approach allows the flux of a given soil surface to be calculated from the increase in radon  
 161 activity concentration  $C_{\text{Rn}}(t)$  within a chamber of known volume during a time  $t$ , as described by Eq. 9:

$$C_{\text{Rn}}(t) = C_0 e^{-\lambda_{\text{eff}} t} + \frac{F \cdot A}{V_{\text{eff}} \cdot \lambda_{\text{eff}}} (1 - e^{-\lambda_{\text{eff}} t}) \quad (9)$$

162

163 where the effective decay constant,  $\lambda_{\text{eff}}$ , is the sum of the radon decay constant ( $\lambda$ ), possible radon lost due to system  
 164 leakages ( $\lambda_l$ ), and radon concentration reabsorbed by the ground ( $\lambda_r$ ), as described by Grossi et al., (2011).  $C_0$  is  
 165 the initial radon activity concentration within the volume,  $V_{\text{eff}}$  is the effective volume where the radon is free to  
 166 accumulate, and  $A$  is the area of the exhaling surface.

167

## 168 2.2. State of the art Exhalation Bed facilities

169

170 Table S1 in the supplementary material presents a summary of EB facilities found in the literature. The Canadian  
 171 Mining Institute (CANMET) built a national reference standard flux bed for calibrating flux monitoring  
 172 instrumentation. This 5 m diameter bed consisted of a 5.5 cm thick layer of uranium bearing material from uranium  
 173 tailings and provided a radon flux of  $285 \pm 41 \text{ mBq m}^{-2} \text{ s}^{-1}$  (Stieff et al., 1996). In the University of South China  
 174 Radon Laboratory a standard facility simulating radon exhalation from soil was built in 2001 (Tan & Xiao, 2011).  
 175 It consisted of a radon source located at the bottom of a conical volume. The middle cylindrical part was made of  
 176 a plaster and spumy board that simulates the soil or sand porosity. Finally, in the upper part, there is powdery  
 177 calcium carbonate to maintain the radon concentration in the conical volume. The reference flux for this system is  
 178  $1482 \pm 50 \text{ mBq m}^{-2} \text{ s}^{-1}$ , which was measured using an activated charcoal box and Lucas cells. It is still operating,  
 179 and some studies continue to use it (Tan & Xiao, 2013; Tan et al., 2020). Oak Ridge Associated Universities  
 180 (Tennessee, USA) constructed a multilayer exhalation bed. It consists of a base layer of uranium ore spread over  
 181 the bottom of a rectangular Hardigg polyethylene case of dimensions  $84 \text{ cm} \times 53 \text{ cm}$ . The base has a 10 cm  
 182 covering layer of dirt to create a uniform flux at the top surface. The reference exhalation rate of this system was  
 183 determined by the accumulation method, using a continuous radon monitor, and by using activated charcoal  
 184 canisters and electrets. The range of values obtained varied from approximately  $80 \text{ mBq m}^{-2} \text{ s}^{-1}$  to  $430 \text{ mBq m}^{-2} \text{ s}^{-1}$   
 185 (Altic, 2014). Onishchenko et al. (2015), from the Institute of Industrial Ecology UB RAS (Ekaterinburg, Russia),

186 designed a calibration system to test radon flux measurement devices. It was constructed from a 200 L metal drum  
187 filled with quartz sand (radium concentration less than 2.5 Bq/kg) with a calibrated  $^{226}\text{Ra}$  source in the bottom  
188 space of the system. The reference exhalation rate obtained by the accumulation method and charcoal canisters  
189 was  $700 \pm 80 \text{ mBq m}^{-2} \text{ s}^{-1}$ .

190 Gutiérrez-Álvarez et al. (2020a; 2020b) performed an experimental characterization of a soil exhalation rate using  
191 the accumulation method (Eq. 9). Two reference exhalation soils were prepared using phosphogypsum in  
192 rectangular polypropylene boxes with 6.0 cm and 13.0 cm soil thicknesses, respectively. Means of the experimental  
193 results of the bed exhalation rates were of  $13.3 \pm 0.4 \text{ mBq m}^{-2} \text{ s}^{-1}$  and  $23.4 \pm 0.5 \text{ mBq m}^{-2} \text{ s}^{-1}$  with an uncertainty  
194 for  $\sigma=1$  of 2%-3%. These previous values were compared to exhalation rates determined by applying the  
195 theoretical approach (Eq. 3) which gave values of  $12 \text{ mBq m}^{-2} \text{ s}^{-1}$  and  $23 \text{ mBq m}^{-2} \text{ s}^{-1}$ , respectively for the two  
196 exhalation beds, with a total uncertainty of about 20%.

197

### 198 **2.3. Design of a Reference Radon Exhalation Bed**

199

200 In the framework of traceRadon, and using information from the previous section, a radon EB was designed and  
201 built at the University of Cantabria (UC) following Gutiérrez-Álvarez et al. (2020a; 2020b). The EB structure  
202 consisted of five stainless steel plates, welded in the shape of a box, open at the top. In this configuration it is  
203 important to minimize air leakages through the plates that may lead to the loss of radon activity. The intended  
204 purpose of this EB was to provide a constant, well characterized, radon emanation rate under a specific set of  
205 controlled laboratory conditions. Since soil moisture influences on the radon emanation were not of specific  
206 interest in this case, a relatively shallow soil matrix was sufficient for the EB aims.

207 The EB structure was filled with a high  $^{226}\text{Ra}$  content soil, extracted from a former Spanish uranium mine in  
208 Saelices el Chico (Spain), managed by the Spanish National Uranium Company ENUSA. A total soil mass of  
209 around 400 kg was collected. The material was then transported to UC laboratory and distributed over a  $30 \text{ m}^2$   
210 plastic surface in a layer of thickness of approximately 1 cm to be dried and homogenized. Soil homogenization  
211 was performed according to technical document 1415 (IAEA, 2004) following these steps: i) the material was  
212 manually homogenized using a stainless-steel rake; and ii) it was sieved with a 2 mm aperture sieve (the device  
213 has a woven wire mesh in accordance with DIN ISO 3310-1). For the sieving process, soil was taken randomly in  
214 5 kg amounts. Finally, the homogenized soil was placed into the EB container.

215 The EB facility was installed in the basement of the UC Faculty of Medicine, in the Laboratory of Environmental  
216 Radioactivity (LaRUC). Sensors were installed to continuously monitor temperature, pressure and soil moisture.  
217 Two thermometers (Testo, Model 175T2) measured the soil temperature and air temperature inside the  
218 accumulation chambers. Soil moisture was measured with an ODYSSEY (Xtreem) probe, and all environmental  
219 parameters were recorded by a data logger every minute. Table S2 of the supplementary material summarizes the  
220 main characteristics of the selected sensors.

221 The EB radon flux was estimated theoretically and experimentally using the approaches presented in Section 2.1.  
222 To apply Eq. 3, the various soil parameters were measured and/or calculated as explained in Section 3. The  
223 experimental derivation of the EB's radon flux was performed using Eq. 9 as by Gutiérrez-Álvarez et al. (2020a).  
224 For this, the whole surface of the EB was covered with a stainless-steel container of known volume (Figure S1 of  
225 the supplementary material). Three radon monitors, an RTM 2200 (Sarad GmbH), a Radon Scout (Sarad GmbH)  
226 and an AlphaE (Bertin Instruments), were used simultaneously to measure the increase of radon concentration  
227 within the effective accumulation volume. Please note that the sum of the volumes occupied by the solid  
228 components of the three monitors were lower than 1% of the total available volume of the accumulation chamber.  
229 In addition, several small air samples were also taken using the grab sampling technique and analysed with the  
230 ionization chamber IK-250 (RADON v.o.s.).

231

### 232 **2.4. State of the art in Radon Flux Systems**

233

234 A literature review carried out in the framework of traceRadon found that radon monitors employed in flux  
235 measurement systems mainly fall into two categories: active or passive. Active monitors analyze the air in real  
236 time, whereas passive monitors (i.e., charcoal canisters) rely on the progressive accumulation of radon by

237 diffusion. The accumulated radon is then measured using a separate system (e.g., by gamma spectroscopy or  
 238 ionization chamber) (McLaughlin, 2011). Due to the need of radon flux systems capable of high-frequency  
 239 measurements (capable of resolving diurnal variability), only active systems will be presented and discussed here.

240 Generally, radon flux systems are comprised of two main parts: a continuous radon monitor and an accumulation  
 241 volume to be placed on the soil surface. The radon flux (or exhalation rate), is then calculated by Eq. 9 using the  
 242 measured increase of radon within the known volume. However, Eq. 9 can only be solved if the exhalation rate  $F$   
 243 and the total system leakage  $\lambda_{eff}$  remain constant over the designated time period. This condition is hard to satisfy  
 244 for long-term radon flux measurements under field conditions, making it difficult to apply the ISO suggested  
 245 exponential fit. Variability of environmental parameters, in the soil and/or atmosphere, may force changes in the  
 246 quantity of radon exhaled from the surface. Furthermore, gradients of temperature and/or pressure between internal  
 247 and external air of the accumulation chamber may change the the leakage of the system ( $\lambda_{eff}$ ). For short  
 248 measurement periods,  $\lambda_{eff} \cdot t \ll 1$  and the initial concentration within the accumulation chamber is relatively close  
 249 to the atmospheric value, which is usually small ( $C_0 \approx 0$ ). Thus, Eq. 9 can be substituted with a Taylor series of  
 250 the exponential truncated to the first order as:

$$C_{Rn}(t) = C_0 e^{-\lambda_{eff} t} + \frac{F \cdot A}{V_{eff} \cdot \lambda_{eff}} (1 - e^{-\lambda_{eff} t}) \approx \frac{F \cdot A}{V_{eff} \cdot \lambda_{eff}} \cdot \lambda_{eff} t = \frac{F}{h_{eff}} \cdot t = b \cdot t \quad (10)$$

251

252 where  $h_{eff} = V_{eff}/A$  is referred to as the effective height of the system (Morawska, 1989). Thus, to minimize radon  
 253 flux and/or  $\lambda_{eff}$  variability during the measurements, it is advisable to perform short radon flux measurements  
 254 which are also important validate radon flux models.

255 The main characteristics of radon flux systems in the literature based on continuous radon monitors are  
 256 summarized here (see Table S3 and Figure S2 of the supplement material for more detail). System 1 was designed  
 257 and built by ANSTO. While not a commercial system, it is based on a commercial AlphaGUARD (AG) monitor  
 258 and has a drum-like accumulation chamber with a lid that can be automatically opened and closed. A separate  
 259 pump is used to circulate air from the accumulation chamber to the AG in a closed loop. No monitoring of the air  
 260 inside the accumulation chamber is performed by this system. System 2 (the *emanometer*), also designed and built  
 261 by ANSTO, is the predecessor of the System 1 and is based on the flow-through accumulation method. In this case  
 262 the accumulation volume is permanently closed and to perform a measurement the edges of the accumulation  
 263 chamber are buried in soil to make a reasonable seal with the emanating surface (Zahorowski and Whittlestone,  
 264 1996). The system has two detection volumes (scintillation cells) separated in the flow path by approximately 5  
 265 minutes to enable separate radon and thoron ( $^{220}\text{Rn}$ ) flux estimation (more details in Zahorowski and Whittlestone,  
 266 1996). System 3 is a commercial accumulation chamber designed and built by LI-COR ([www.licor.com](http://www.licor.com)). To date,  
 267 this chamber is only sold together with an 8100-401 Chamber Control Kit for the purpose of automatic  $\text{CO}_2$  flux  
 268 measurements. So far it has never been coupled with any commercial radon monitor. Systems 4, 5 and 6 are  
 269 research products, each using different radon monitors and types of accumulation chambers, some of which can  
 270 be opened and closed automatically. System 6, in particular, developed at the Helmholtz Zentrum München  
 271 (Institute of radiation protection), Neuherberg, Germany, allows radon flux measurements to be made at different  
 272 sites around a circular path, using a mechanical arm (Yang et al., 2017). Unfortunately, system 6 is no longer  
 273 available due to the discontinuation of the research group. Systems 7 and 8, built by INTE-UPC and UC  
 274 respectively, are based on radon monitors (DOSEman and AlphaE) operating in diffusion mode. Radon monitors  
 275 operating in diffusion mode can influence the flux instrument's response time, as well as the subsequent fit  
 276 calculation for estimating the flux, as will be shown in Section 3. Both systems have accumulation chambers that  
 277 can only be opened manually, but air is refreshed by an external pump.

278 The importance of the accumulation chamber characteristics when measuring soil gas fluxes should not be  
 279 underestimated. An inherent challenge in flux chamber design is minimizing the influence that the chamber may  
 280 have on the measurements, especially for long-term observations. Based on our literature review, the main  
 281 characteristics required for radon flux systems (monitors and accumulation chambers) are listed and have been  
 282 taken into account when developing a radon flux system suitable for use as a Transfer Standard.

283 For a system capable of making radon flux measurements at high temporal resolution, which minimizes the  
 284 disturbance of flux estimates by changing environmental parameters inside the accumulation chamber, the main  
 285 requirements are:

- 286 - to use a continuous direct radon monitor that measures activity concentration in flow mode (not diffusion
- 287 mode) at a high temporal resolution (e.g., 1 min - 10 min), and with a minimum detectable radon activity
- 288 concentration low enough to measure short term radon increases within the accumulation chamber with
- 289 a statistical uncertainty lower than 20%, allowing radon flux measurements to be obtained using Eq. 10.
- 290 - the accumulation chamber needs to open completely and automatically after each measurement period,
- 291 to establish the initial condition of  $C_0$  equal to the ambient radon concentration.
- 292 - environmental sensors are needed inside and outside the accumulation chamber.
- 293 - the accumulation chamber needs to have a smooth internal geometry to avoid inhomogeneous internal
- 294 concentration distribution.
- 295 - the accumulation chamber should be painted gloss white, to minimize the temperature difference between
- 296 air inside and outside of the chamber when the chamber is in direct sunlight.
- 297 - the chamber should have a matching collar to attach to (via an easy to clean and seal flange), which can
- 298 be firmly seated in the soil (to a depth of 2 cm – 10 cm, depending on soil type / texture) to minimize
- 299 radon losses (Gutiérrez-Álvarez et al., 2020b).

300

## 301 **2.5. Design of a new Radon Flux Transfer Standard (TS) System**

302

303 Based on the monitor requirements described in section 2.4 an automatic and low maintenance radon flux  
 304 measurement system was designed and built at ANSTO in September 2020 as an alternative implementation of  
 305 System 1, described previously. This new system was implemented in collaboration with the UPC, and  
 306 subsequently fully characterized by UPC in collaboration with UC, in the framework of traceRadon. UPC also  
 307 implemented the means to remotely control the system for data download during the experiments and improved  
 308 the scripts for the flux calculations and analysis.

309 This instrument enables 8 automatic flux measurements to be performed each day, every 3 hours. The *AutoFlux* is  
 310 comprised of an AG PQ2000 PRO (Saphymo) radon monitor (working in 10 min flow mode), an accumulation  
 311 chamber (drum) with automatic lid, and several environmental sensors installed within the soil, inside the drum,  
 312 and outside the drum at 50 cm above ground level. An internal lip near the bottom of the accumulation chamber  
 313 allows the chamber to be pushed 5 cm into the soil to make a good seal with the surface. The radon flux is estimated  
 314 by performing linear fit of the radon concentration increase within the closed drum every 10 min over a 1-hour  
 315 period using Eq. 10. The drum's hinged lid is opened and closed using a 150 lb 4" classic rod linear actuator. The  
 316 actuator is fitted with an external limit switch kit, powered by a 4 x 12V DC relay card and controlled by a CSI  
 317 CR1000 datalogger (<https://www.campbellsci.es/cr1000>). The opening (default 2h) and closing (default 1h) times  
 318 of the accumulation chamber are adjustable and controlled by the program in the datalogger.

319 The novelty of this system is that the diurnal and seasonal variability of soil radon fluxes can be observed and  
 320 studied in parallel with measurements of soil properties and meteorological conditions. The *AutoFlux* system was  
 321 constructed in such a way that it can perform long-term measurements of radon flux and environmental parameters  
 322 with almost zero maintenance requirements. Unfortunately, this system does not provide a movable arm to allow  
 323 a periodic change of the measurement spot. Consequently, the positioning of the lid, even when fully open, can  
 324 sometimes partially shelter the measurement surface from the rainfall that the surrounding surface is receiving. To  
 325 best match conditions inside and outside of the chamber when open, the accumulation chamber should be  
 326 positioned such that the lid opens into the direction of the sun at midday, to maximise the sunlight received by the  
 327 surface inside.

328 Figure 1 shows the *AutoFlux* system during a typical radon flux field measurement. Figure S3 of the supplementary  
 329 material presents a simplified scheme of the actual state of the *AutoFlux* system.

330



331

332 **Figure 1. Image of the *AutoFlux* system running in the field. The radon activity concentration, internal air temperature,**  
 333 **differential pressure and soil characteristics are measured within the white drum. Ambient temperature, humidity,**  
 334 **pressure and rainfall are measured on the side of the transport case (~50 cm a.g.l.), and the main system components**  
 335 **are located inside the waterproof transport case.**

336 The air exhaled from the soil, rich in radon and thoron ( $^{220}\text{Rn}$ ), enters the accumulation nominal volume  $V_D = 0.02$   
 337  $\text{m}^3$  and is pumped at  $Q = (1 \pm 0.1) \text{ L min}^{-1}$  first through a filter (PALL Acro 50) and then through a Permapure PD  
 338 gas dryer, intended to maintain humidity levels below saturation conditions within the AG monitor. The low  
 339 humidity air stream then enters a delay volume ( $V_{Th} = 6 \cdot 10^{-3} \text{ m}^3$ ) within which the ambient thoron decays. Next,  
 340 the air passes into the detection volume of the AG ( $V_{AG} = 0.62 \cdot 10^{-3} \text{ m}^3$ ) where the radon concentration is measured  
 341 with a 10-minute temporal resolution. The total volume of the circuit tubes is  $V_{Tubes} \approx 0.3 \cdot 10^{-3} \text{ m}^3$ . The area of the  
 342 exhaling surface is  $A = 0.126 \text{ m}^2$ . Considering the total volume where the radon concentration will be accumulating  
 343  $V_{eff}$  will be in this case equal to  $V_{tot} = V_D + V_{Th} + V_{AG} + V_{Tubes} = 2.6 \cdot 10^{-3} \text{ m}^3$  the effective height  $h_{eff}$  in the Eq. 10 is  
 344 equal to 0.204 m.

345 The drum and soil sensors are installed directly into the soil. All sensor outputs are read by a CR1000 datalogger.  
 346 A Raspberry Pi 4 (RPI) enables scheduled data downloads from both the CR1000 datalogger and AG via a RS232  
 347 serial port and serial to USB FTDI adapter. The RPi, AG, datalogger, PD and all electronic components of the  
 348 *AutoFlux* system are safety located within a sturdy, waterproof transport case. External sensors are installed on the  
 349 outer walls of the blue transport case. Table 1 summarizes the sensors installed within the *AutoFlux* system. Data  
 350 stored on the RPi, which are downloaded from the AG and datalogger hourly, can be transferred to a notebook  
 351 computer by connecting the RPi with an Ethernet cable, assuming a Bitwise SSh Client is installed.

352 Figure S4 of the supplementary material shows the accumulation chamber of the *AutoFlux* system in its closed  
 353 state (left side) and opened state (right side) during a typical radon flux measurement.

354

355

356

**Table 1. Sensors installed within the *AutoFlux* system.**

<b>Variable (Label within the document)</b>	<b>Sensor</b>	<b>Location</b>	<b>Unit (S.I.)</b>	<b>Picture</b>
Volumetric Water Content (VWC) in the soil	CSI CS655 Water Content Reflectometer	Inside Drum	$\text{m}^3/\text{m}^3$	
Electrical conductivity (EC) soil	CSI CS655 Water Content Reflectometer	Inside Drum	dS/m	-

Water vapor pressure (VaporPress)	CSI CS655 Water Content Reflectometer	Inside Soil	kPa	-
Soil temperature (T)	CSI CS655 Water Content Reflectometer	Inside Soil	°C	
Drum air temperature (DrumTemp)	SDI-12 sensor Unidata 6508A	Inside Drum	°C	
Atmospheric air Pressure (AtmPress)	Integrated ATMOS-14 sensor	Outside attached to box	mbar	
Ambient air Temperature (AirTemp)	Integrated ATMOS-14 sensor	Outside attached to box	°C	-
Relative Humidity (RH)	Integrated ATMOS-14 sensor	Outside attached to box	%	-
Accumulated rain (Rain)	Hydreon RG-11 Optical Rain Gauge	Outside Drum	mm	
Differential pressure between Drum and external atmosphere (DiffPress)	Novus NP785	Inside/Outside Drum	Pa	

357

358 **2.6. Calibration of a secondary Radon Flux System using the *AutoFlux* and the UC EB facility**

359

360 After the characterization of the EB (see Section 3.1), and the calibration of the TS under stable laboratory  
361 conditions with a constant reference radon flux (see Section 3.2), they were used together to calibrate a second  
362 radon flux system (*INTE\_flux*, system 6 of Section 2.3).

363 The *INTE\_flux* system also operates continuously and is capable of making 3 radon flux measurements per day. It  
364 consists of a cylindrical metallic chamber connected to two electro valves and a pump. The electro valves and  
365 pump are controlled using a Programmable Logic Controller (PLC) and the system is powered via a 30 m water-  
366 proof cable. To measure a radon flux with this system, the <sup>222</sup>Rn concentration in the chamber exhaled from the  
367 soil surface is continuously measured using a DOSEman monitor in diffusion mode, which was previously  
368 calibrated at the Radon Reference Chamber (secondary) of the INTE-UPC in agreement with the IEC 61577-4.  
369 The DOSEman monitor is powered by an internal battery that lasts 15 days.

370 A typical calibration experiment setup, as carried out at the UC EB facility, is shown in Figure 2, where the  
371 *INTE\_Flux* and TS were installed on the EB between the 29<sup>th</sup> of June 2021 and 1<sup>st</sup> of July 2021.



372

373 **Figure 2. Typical calibration experiment carried out at the UC laboratory: the *INTE\_Flux* system is installed together**  
 374 **with the TS system on the EB facility.**  
 375

### 376 **3 Results**

377

#### 378 **3.1. Characterization of the Radon Exhalation Bed (EB) facility**

379

380 The EB radon flux was determined under laboratory conditions at specific points in time using both theoretical  
 381 and experimental approaches, as explained in Section 2.1. The necessary parameters to apply Eq. 3 were measured  
 382 and/or calculated as explained later in this section and are presented in Table 2, along with their respective  
 383 uncertainties (with  $k=1$ ). Table 2 also presents all variables and parameters measured or calculated for the  
 384 experimental characterization of the EB within a week of its installation, together with values obtained from the  
 385 literature ( $D$  and  $\lambda$ ).

##### 386 **3.1.1 Radium activity concentration ( $C_{Ra}$ )**

387

388 The average radium activity concentration of the soil in the EB was obtained by gamma spectrometry analysis of  
 389 5 separate samples. The samples were extracted from the center and each of the four corners of the EB at a depth  
 390 of 10-15 cm. Samples were hermetically sealed in a cylindrical container for one month to allow the  $^{226}\text{Ra}$  to reach  
 391 secular equilibrium with its short-lived progeny ( $^{214}\text{Pb}$  and  $^{214}\text{Bi}$ ). After this time, the radium activity was  
 392 determined using the  $^{214}\text{Pb}$  photopeak (351.93 keV) with a high-resolution gamma HPGe coaxial detector (model  
 393 GL-2015-7500, Canberra, USA) following Celaya et al., (2018). The mean  $^{226}\text{Ra}$  activity concentration was  $19130$   
 394  $\pm 350$  Bq  $\text{kg}^{-1}$ .

##### 395 **3.1.2 Emanation factor ( $\epsilon$ )**

396

397 The initial emanation factor,  $\epsilon_0$  of the EB soil was obtained by measuring the ratio between the radon activity ( $A_{Rn}$ )  
 398 within the pores of a small, thin ( $< 5\text{mm}$ ) soil sample and its radium activity ( $A_{Ra}$ ) (Eq. 2).  $A_{Rn}$  in a  $M = 100$  g soil  
 399 sample was measured by Eq. 9 after hermetically sealing the sample within a volume  $V = 0.024$   $\text{m}^3$  and making an  
 400 exponential approximation of the radon concentration increase with time. The experiment was repeated  $n = 3$   
 401 times.

402 Each experiment was run over a period of 500 hours and was replicated at standard temperature conditions ( $T =$   
 403  $298$  K) with a dried soil sample. A continuous radon monitor (Radon Scout; Sarad GmbH) was used for these tests  
 404 after being calibrated in the LaRUC radon chamber (Fuente et al., 2018). A final average emanation factor was  
 405 obtained as:

$$\epsilon_0 = \frac{A_{Rn}}{A_{Ra}} = \frac{\phi}{\lambda_{eff} \cdot C_{Ra} \cdot M} = \frac{0.032 \cdot 0.024}{2.2 \cdot 10^{-6} \cdot 19130 \cdot 0.1} = 0.18 \quad (11)$$

406

407 with  $\phi$  the activity rate of radon ( $\text{Bq s}^{-1}$ ) obtained as the mean of the three exponential fits and  $\lambda_{eff} = (2.2 \pm$   
 408  $0.3) \cdot 10^{-6} \text{ s}^{-1}$ , the effective decay constant of the system. The estimated uncertainty of the mean of the initial  
 409 emanation factor was determined from the standard deviation of the three experiments and it was equal to  
 410 0.03. It can be observed that  $\lambda_{eff} \approx \lambda$ , the decay constant of radon, ensuring negligible leakages within the system.  
 411 A typical measurement experiment is shown in Figure S5 of the supplementary material.

412 As mentioned in the introduction, the emanation factor could vary over time because – apart from the grain size –  
 413 it also depends on the moisture content and temperature of the material. Zhuo et al., (2006) and Zhuo et al., (2008)  
 414 investigated the relationship between the emanation factor variability with soil moisture and soil temperature, and  
 415 derived the following empirical relationship Eq. 12:

$$\varepsilon = \varepsilon_0 \cdot [1 + a(1 - e^{-bw_s})] \cdot [1 + c(T - 298)] \quad (12)$$

416 where  $\varepsilon$  is the radon emanation factor estimated for a given temperature  $T$ , and  $\varepsilon_0$  is the radon emanation factor  
 417 measured at a temperature of  $T = 298 \text{ K}$  for dried soil (see Eq. 11).  $w_s$  is the water saturation fraction and  $a, b, c$   
 418 are parameters calculated for different types of soil textures and declared by Zhuo et al., (2008).  
 419

### 420 3.1.3 Bulk density ( $\rho$ )

421  
 422 The soil bulk density  $\rho$  was calculated by measuring the mass,  $M$ , with a calibrated balance, and dividing this by  
 423 its volume,  $V_s$ . The volume was measured from an undisturbed soil sample using a test tube manufactured  
 424 according to ISO 4788. A value of  $1645 \pm 2 \text{ kg m}^{-3}$  was calculated.

### 425 3.1.4 Radon diffusion length ( $L$ )

426 As explained in Section 2, to simplify Eq. 1 to Eq. 3 the soil thickness  $z$  of the EB needs to be much smaller than  
 427 the radon diffusion length  $L$  in the material. Equations 4 to 7 had to be applied after measuring and/or calculating  
 428 the required soil parameters for these equations: water saturation ( $w_s$ ) and porosity ( $p$ ) of the soil. In addition, to  
 429 apply Eq. 6 and 7 the grain density and water content of the soil sample had to be measured. The mass water  
 430 content  $w_c$  ( $\text{kg/kg}$ ) can be measured as the ratio of the mass of water and the mass of dry soil. It is measured by  
 431 weighing a soil sample,  $m_{wet}$ , then drying the sample to remove the water and weighing it again,  $m_{dry}$ :

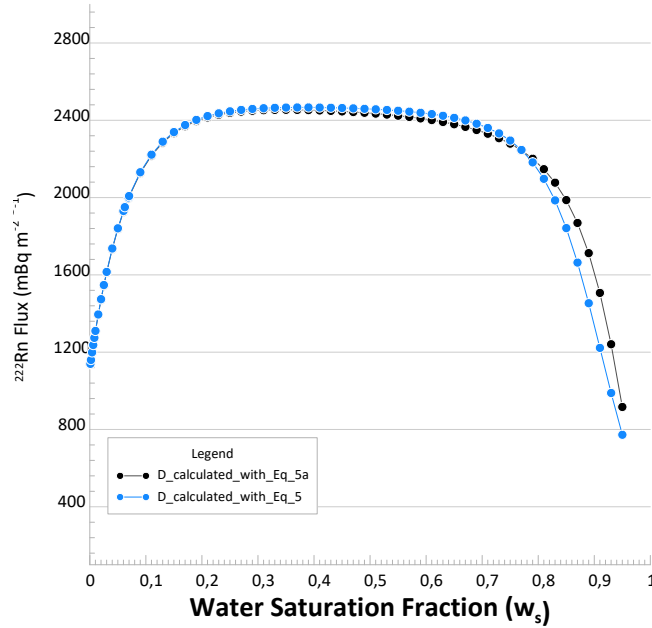
$$w_c = \frac{m_{wet} - m_{dry}}{m_{dry}} \quad (13)$$

432 The grain density  $\rho_g$  is the ratio of the mass of a dry sample and its volume after eliminating the contribution of  
 433 the interparticle void volume. It can be calculated from the sample weight  $m_{dry}$  and the volume  $V_{dry}$  of dry soil  
 434 from:

$$\rho_g = \frac{m_{dry}}{V_{dry}} \quad (14)$$

435  
 436 The diffusion coefficient  $D$  and the diffusion length  $L$  can now be calculated using Eq. 4 and 5 and  $L$  is equal to  
 437  $(1.286 \pm 0.015) \text{ m}$ . The measured EB thickness is equal to  $(0.165 \pm 0.005) \text{ m}$ , thus the hypothesis  $z \ll L$  is verified.  
 438 Using all the previous parameters the radon flux from the EB can be theoretically estimated by Eq. 3 and it is  
 439  $F_{Th\_EB} = 1918 \pm 278 \text{ mBq m}^{-2} \text{ s}^{-1}$ .

440 Figure 3 shows the theoretical radon flux of the EB calculated using Eq. 1 assuming that the emanation factor  
 441 varies according to Eq. 11 of Zhuo et al., (2008). The two versions of radon flux presented in Figure 3 represent  
 442 changes in the adopted diffusion coefficient  $D$ . In one case the flux has been calculated using  $D$  from Eq. 5 (blue  
 443 dots) and the other,  $D$  from Eq. 5a (black dots). It is evident that no significant difference in EB flux estimate was  
 444 observed between these methods in the range of water saturation values for which the EB characterization was  
 445 performed.



446

447 **Figure 3. Variability of EB  $^{222}\text{Rn}$  flux calculated using Eq. 1 where the emanation factor variability follows Eq. 11 and**  
 448 **the diffusion coefficient  $D$  was estimated using both Eq. 5 (black dots) and Eq. 5a (blue dots).**

449

450 As explained in the Methods section, an empirical evaluation of the EB radon flux was also undertaken by  
 451 enclosing the whole exhaling surface with a cover of known volume. The experiments were performed using  
 452 different radon monitors inside the closed volume to monitor the radon buildup. Figure S6 of the supplementary  
 453 material shows the results of a typical accumulation experiment to estimate the EB radon exhalation rate. The  
 454 experiment was repeated several times to confirm its reliability. The response time of the RTM device was set to  
 455 1 minute, while it was 10 minutes for the Radon Scout and AlphaE. Air samples were also collected from the  
 456 enclosed volume every 15 minutes for independent analysis. Radon concentrations inside the volume reached  
 457 values of about  $130 \text{ kBq m}^{-3}$  after only 5 hours. The diffusion mode of operation for the AlphaE and Radon Scout  
 458 monitors (green and orange dots, respectively in Figure S6) is not capable of correctly representing the temporal  
 459 variability of radon within the volume, so data from these devices were not used to estimate the EB radon  
 460 exhalation rate.

461 The radon exhalation rate was obtained by applying Eq. 10 using parameters summarised in Table 2 (bottom part).  
 462 Mean values observed by the environmental sensors of the EB facility during the experiments are also reported.  
 463 The mean of the experimntal radon flux was  $F_{\text{exp\_EB}} = 1757 \pm 67 \text{ mBq m}^{-2} \text{ s}^{-1}$ .

464

465 **Table 2. Results of the parameters/variables influencing the calculation/measurements of radon flux from the**  
 466 **Exhalation Bed configuration for the theoretical and experimental approaches, respectively. Uncertainties are**  
 467 **expressed without any coverage factor ( $k=1$ ).**

Parameter	Symbol	Result
Emanation factor	$\varepsilon$	$0.18 \pm 0.03$
Radium concentration	$C_{\text{Ra}}$	$(19130 \pm 350) \text{ Bq kg}^{-1}$
Bulk density	$\rho$	$(1645 \pm 2) \text{ kg m}^{-3}$
Grain density	$\rho_g$	$(2570 \pm 38) \text{ kg m}^{-3}$
Thickness	$z$	$(0.165 \pm 0.005) \text{ m}$
Mass Water content	$w_c$	$(0.0132 \pm 0.0004) \text{ kg/kg}$
Water saturation	$w_s$	$(0.061 \pm 0.008) \text{ m}^3/\text{m}^3$
Porosity	$p$	$0.3599 \pm 0.0001$
Diffusion coefficient	$D$	$(3.47 \pm 0.08) \cdot 10^{-6} \text{ m}^2/\text{s}$
Diffusion length	$L$	$(1.286 \pm 0.015) \text{ m}$
Radon decay constant	$\lambda$	$2.0993(1) \cdot 10^{-6} \text{ s}^{-1}$

Parameter/Variable	Symbol	Result
$^{222}\text{Rn Flux}$	$F_{Th\_EB} \pm U_{Th\_EB}$	$1918 \pm 278 \text{ mBq m}^{-2} \text{ s}^{-1}$
Effective height	$h_{eff}$	$(0.225 \pm 0.005) \text{ m}$
Air temperature	$T$	$(20.7 \pm 0.3) \text{ }^\circ\text{C}$
Mass water content in mass	$w_c$	$(0.013 \pm 0.001) \text{ kg/kg}$
Air moisture	$RH$	$(47.0 \pm 0.7)\%$
$^{222}\text{Rn Flux}$	$F_{Exp\_EB} \pm U_{Exp\_EB}$	$1757 \pm 67 \text{ mBq m}^{-2} \text{ s}^{-1}$

468

469

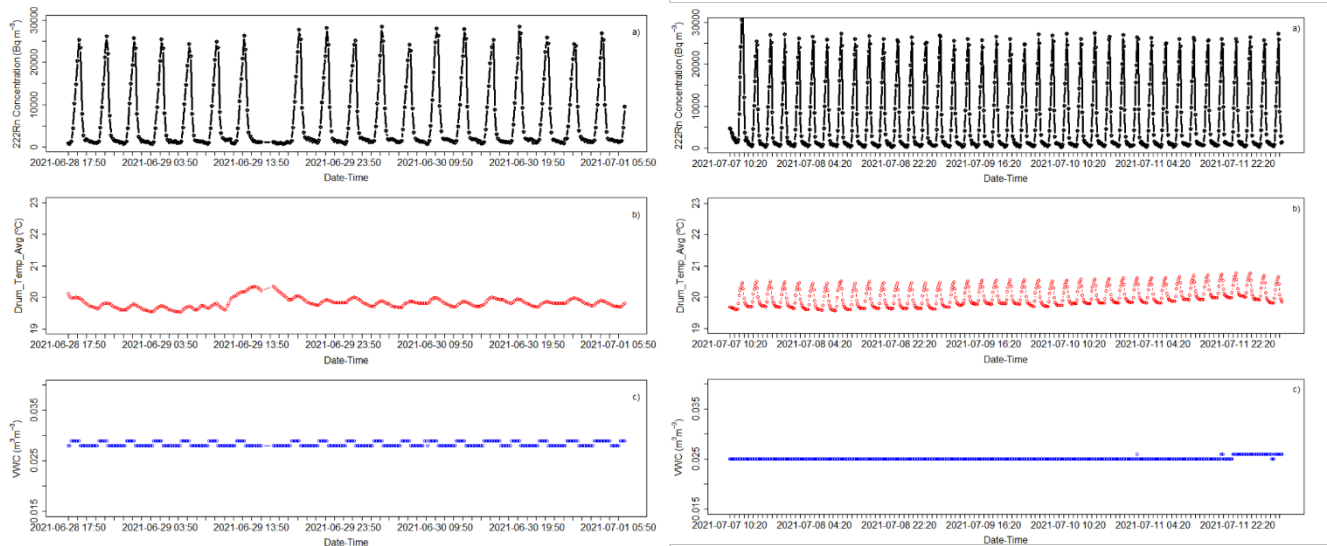
470

### 3.2 Characterization of the Radon Flux Transfer Standard (TS) System

471 The *AutoFlux* was characterized and calibrated under controlled laboratory conditions using the EB facility as  
472 described previously. Figure S7 of the supplementary material shows the *AutoFlux* setup for a typical laboratory  
473 measurement at UC. Two laboratory experiments were performed at standard environmental conditions: i) from  
474 the 28<sup>th</sup> of June 2021 to the 1<sup>st</sup> of July 2021 (19 radon flux measurements); and ii) from the 7<sup>th</sup> to the 12<sup>th</sup> of July  
475 2021 (39 radon flux measurements). Figure 4 shows the radon activity concentrations (upper panels) measured by  
476 the *AutoFlux*'s AG during the two continuous experiment periods for each accumulation hour. The bottom panels  
477 of Figure 4 show the soil Volume Water Content (*VWC*) time series measured by the CSI CS655 Water Content  
478 Reflectometer and the air temperature inside the drum measured by the SDI-12 (Unidata 6508A) sensor during  
479 these experiments. A constant increase of around  $28 \cdot 10^3 \text{ Bq m}^{-3}$  of radon and of  $1 \text{ }^\circ\text{C}$  of temperature was measured  
480 during the 1 h accumulation phase within the system. The Volume Water Content (*VWC*) measured during the  
481 two experiments ranged between  $0.025 \text{ m}^3/\text{m}^3$  and  $0.029 \text{ m}^3/\text{m}^3$ .

482

483



484

485 **Figure 4. Radon activity concentrations (black dotted lines in panel a) measured by the *AutoFlux*'s AG during the two**  
486 **calibration experiments. The bottom panels show the time series of the soil *VWC* (blue dotted lines in panel c) and air**  
487 **temperature inside the drum (red dotted lines in panel b) during the experiments.**

488 An example of the increase in radon activity concentration measured by the *AutoFlux*'s AG during a typical 1h  
489 accumulation period for a single flux measurement is shown in Figure 5. It is evident that the first two values after  
490 the chamber closes (0 and 1 in Fig. 5) do not follow the expected theoretical linear increase from Eq. 10. Including  
491 these values in the slope calculation could lead to an underestimation of the flux. To better understand the process  
492 going on within the drum during a measurement, it is important to note that the 10-minute AG data are  
493 representative of the mean radon activity concentration measured over that period, and that the timestamp assigned  
494 to each recorded value is at the end of each measurement period. Consequently, the first output value after the  
495 chamber is closed (0 in Fig. 5) actually represents the mean radon concentration measured over the 10-minute

496 period leading up to the point of closure. This value has therefore not been considered for the experimental linear  
 497 fit analysis.

498 A box model (Eq. 15, 16 and 17 and Figure S8 of the supplementary material) can be used to better understand the  
 499 behavior of radon activity concentrations in the *AutoFlux* system during the hour of accumulation. Figure S8 shows  
 500 the three main volumes of the system:  $V_{AG}$  is the AlphaGUARD detection volume;  $V_D$  is the drum (accumulation  
 501 chamber) volume and  $V_u$  is the total volume of all tubing ( $V_{tubes}$ ) plus the thoron delay volume ( $V_{Th}$ ). The change  
 502 in radon concentration with time in each volume of the system components can be described by the following set  
 503 of differential Equations:

504

$$\frac{dC_D(t)}{dt} = \frac{F \cdot A}{V_D} - C_D(t) \cdot \frac{Q}{V_D} + C_{AG}(t) \cdot \frac{Q}{V_{AG}} \quad (15)$$

505

$$\frac{dC_u(t)}{dt} = C_D(t) \cdot \frac{Q}{V_D} + C_u(t) \cdot \frac{Q}{V_u} \quad (16)$$

506

$$\frac{dC_{AG}(t)}{dt} = C_u(t) \cdot \frac{Q}{V_u} + C_{AG}(t) \cdot \frac{Q}{V_{AG}} \quad (17)$$

507

508 Equations 15, 16 and 17 do not take into account the decay of the radon within these volumes because its will be  
 509 negligible during the 1h accumulation experiment length. Figure S9 of the supplementary material shows the  
 510 theoretical increase of radon concentration with time in each of the respective volumes  $C_D$  (drum concentration),  
 511  $C_u$  (concentration in thoron delay and tubes) and  $C_{AG}$  (concentration in the AG) during the first hour of system  
 512 closure, obtained through the analytical solution of Eq. 15, 16 and 17 with the software Mathematica (Wolfram  
 513 Mathematica). The observed increase in radon within the AG becomes parallel to the radon increase within the  
 514 accumulation chamber only after 700 sec ( $\approx 12$  minutes). Therefore, the second value measured by the AG after  
 515 the accumulation volume is closed (point 1 in Figure 5) also can't be considered as part of the experimental linear  
 516 fit analysis due to the system response time delay.

517 Looking at Figure 5, the slope of the experimental data (black dotted line) during the accumulation hour, ignoring  
 518 the first two points (0 and 1) for the reasons mentioned above, gives a radon flux of  $(1899 \pm 60)$  mBq m<sup>-2</sup> s<sup>-1</sup>  
 519 according to Eq. 10, where the associated uncertainty is calculated from the residual standard error (rse) of the  
 520 linear fit. These data were measured with a mean volume water content  $w_v$  of 0.025 m<sup>3</sup>/m<sup>3</sup>, equal to a soil water  
 521 saturation  $w_s = 0.069$  m<sup>3</sup>/m<sup>3</sup> that, according to Eq. 1 and 11, gives a theoretical radon flux of  $(1974 \pm 277)$  mBq  
 522 m<sup>-2</sup> s<sup>-1</sup>. Finally, the experimental data (black dotted line in Figure 5) were fitted with theoretical data (blue dotted  
 523 line in Figure 5) obtained by solving differential equations 15, 16 and 17 with a radon flux of about ( $F_{Th\_AF} = 1871$   
 524  $\pm 187$ ) mBq m<sup>-2</sup> s<sup>-1</sup> where the uncertainty of 10% (k=1) is due to the volume estimations and flow variability during  
 525 the accumulation hour. All of these results are consistent if the associated uncertainties are taken into account and  
 526 support the understanding of the system response.

527 Radon concentration time series obtained by exposing the *AutoFlux* system to the UC EB facility (Experiments I  
 528 and II in Figure 4) were analyzed and Eq. 10 was used to calculate the radon fluxes for each measurement, using  
 529 only points 2, 3, 4, 5 and 6 of the accumulation phase. This resulted in a mean radon flux of  $F_{Exp\_AF} = 1856$  mBq  
 530 m<sup>-2</sup> s<sup>-1</sup> with a standard deviation of  $\sigma_{Autoflux} = 86.5$  mBq m<sup>-2</sup> s<sup>-1</sup> over a total of n = 58 radon flux measurements.

531 The error of the mean of the flux measured experimentally by the *Autoflux* monitor will be  $u_{Autoflux} = \frac{\sigma_{Autoflux}}{\sqrt{n}} =$   
 532 11.4 mBq m<sup>-2</sup> s<sup>-1</sup>. All results are consistent within their respective uncertainties. Finally, Table 3 summarizes the  
 533 mean radon flux measured by the *AutoFlux* system during experiments I and II at the UC EB facility in October  
 534 2021. The means and standard deviations of the variables measured by the *AutoFlux* environmental sensors are  
 535 also reported.

536

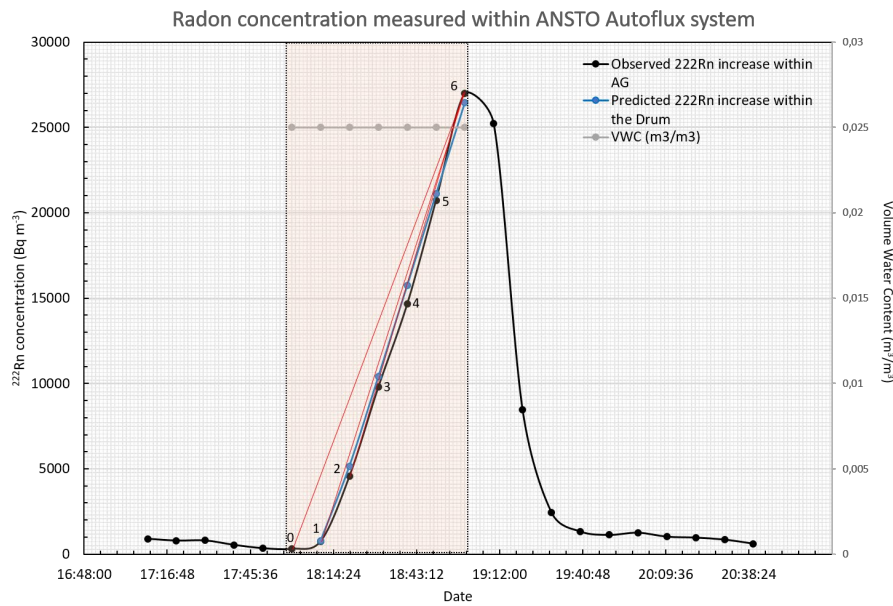
537

538

539 **Table 3. Results of  $^{222}\text{Rn}$  fluxes and environmental parameters calculated and/or measured using the *AutoFlux* system**  
 540 **during experiments I and II carried out at the UC facility in October 2021 (Grey shaded values have been calculated**  
 541 **using Eq. 10 and 15-16-17).**

Variable	Mean	St. Dev.
$F_{Exp\_AF}$ ( $\text{mBq m}^{-2} \text{s}^{-1}$ )	1856	86.5
$F_{Th\_AF}$ ( $\text{mBq m}^{-2} \text{s}^{-1}$ )	1871	187
Flow ( $\text{L min}^{-1}$ )	0.91	0.01
VWC ( $\text{m}^3/\text{m}^3$ )	0.025	0.002
AirTemp ( $^{\circ}\text{C}$ )	19.92	0.095
RH (%)	69.91	1.58
AtmPress (mbar)	1015.3	2.5
DrumTemp ( $^{\circ}\text{C}$ )	20.04	0.11

542



543

544 **Figure 5. Increase in radon activity concentration within the *Autoflux*'s accumulation chamber during a typical radon**  
 545 **flux measurement (black dotted line). Blue dotted line represents the theoretical value calculated within the AG volume.**  
 546 **The grey dots indicate the *VWC* measured in the soil at the same time. Red lines show different slopes obtained when**  
 547 **considering different values.**

548

549 Considering the agreement between the theoretical and experimental results of the mean radon flux values obtained  
 550 directly from the EB ( $F_{Th\_EB}$  and  $F_{Exp\_EB}$ ) or using the *Autoflux* on the EB ( $F_{Th\_AF}$  and  $F_{Exp\_AF}$ ), the calibration factor  
 551 of the *AutoFlux* monitor can be now calculated as  $F_{Cal\_Autoflux} = F_{Exp\_EB}/F_{Exp\_AF} = 0.95$ . The uncertainty of the  
 552 calibration factor  $u_{Cal\_Autoflux} = 0.07$ , calculated following the 'Guide to the Expression of Uncertainty in  
 553 Measurement' (JCGM 100) by Eq. 18:

$$554 \left( \frac{u_{Cal\_Autoflux}}{F_{Cal\_Autoflux}} \right)^2 = \left( \frac{u_{Autoflux}}{F_{Autoflux}} \right)^2 + \left( \frac{u_{Exp\_EB}}{F_{Exp\_EB}} \right)^2 + \left( \frac{u_{F\_Corr}}{F_{Corr}} \right)^2 \quad (18)$$

555 It should be noted that  $F_{Exp\_EB}$  and  $F_{Exp\_AF}$  were measured within a 1% of variability of the water saturation  
 556 condition of the emanating soil, which could induce up to a 6% of variability on the measured flux. This possible  
 557 variability should be considered within the calculation of the uncertainty of the calibration factor of the Transfer  
 558 Standard monitor, including a correction factor  $F_{Corr} = 1$  with an uncertainty  $u_{F\_Corr} = 0.06$ .

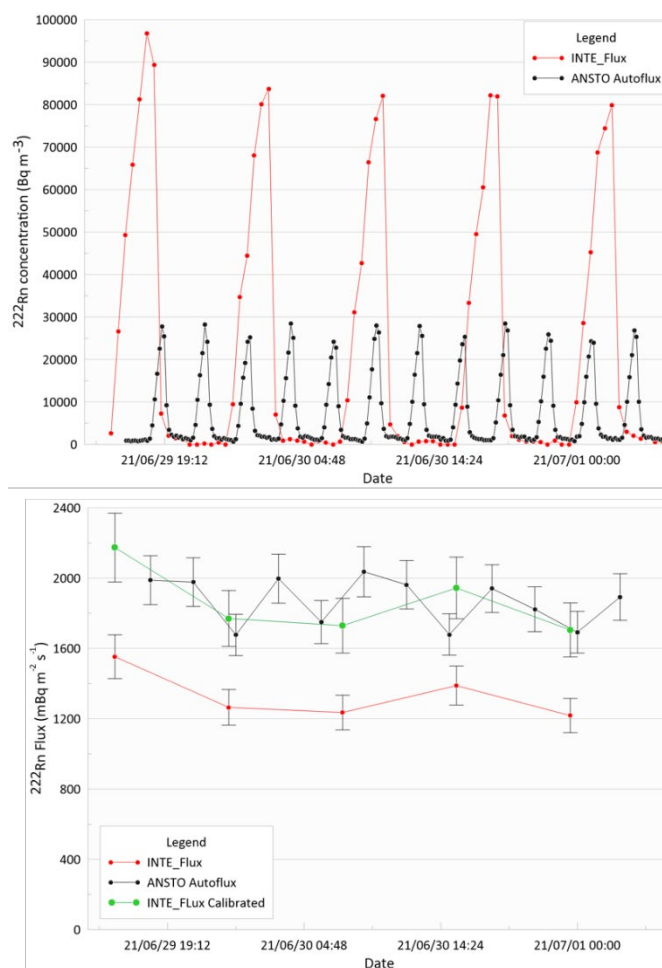
559

560 **3.3. Calibration of the INTE\_Flux system using the TS and the EB facility**

561

562 The upper panel of Figure 6 shows the radon concentration time series measured at the same time by the DOSEman  
 563 included within the accumulation chamber of the *INTE\_Flux* system and by the AG used for the *AutoFlux* system.  
 564 The slope  $b$  in Eq. 10 can be calculated for each radon accumulation period of the *INTE\_Flux* and it has been  
 565 reported in Table 4, together with the radon fluxes measured by the *INTE\_Flux* when a nominal  $h_{eff} = 0.15$  m is  
 566 applied. The mean value of the radon flux calculated using the *INTE\_Flux* system was  $F_{Client} = 1332$  mBq m<sup>-2</sup> s<sup>-1</sup>  
 567 with a standard deviation of  $\sigma_{Client} = 140$  mBq m<sup>-2</sup> s<sup>-1</sup> and the standard error of the mean  $u_{Client} = \frac{\sigma_{Client}}{\sqrt{n}} = 63$  mBq  
 568 m<sup>-2</sup> s<sup>-1</sup>, where  $n = 5$ , the number of radon flux measurements carried out with the *INTE\_Flux* system. The mean of  
 569 the radon flux measured by the TS instrument (*AutoFlux*) during the same period was  $F_{Ref} = 1868$  mBq m<sup>-2</sup> s<sup>-1</sup> with  
 570 a standard deviation of  $\sigma_{Ref} = 137$  mBq m<sup>-2</sup> s<sup>-1</sup> and a standard error of the mean  $u_{Ref} = 39.5$  mBq m<sup>-2</sup> s<sup>-1</sup> ( $n_{Ref} = 12$ ).  
 571 The calibration factor of the *INTE\_Flux* system can be estimated as  $F_{Cal} = F_{Ref\_Cal}/F_{Client} = 1.33$ , where  $F_{Ref\_Cal} =$   
 572  $F_{Ref} \cdot F_{Cal\_Autoflux}$  represents the calibrated radon flux value obtained by the ANSTO *Autoflux* system over the  
 573 experiment.

574  
 575  
 576



577  
 578  
 579 **Figure 6. Upper Panel: Time series of radon concentrations measured by the DOSEman (output each 30 min) in the**  
 580 ***INTE\_Flux* system accumulation chamber and by the AG (output each 10 min) used for the *AutoFlux* on the EB facility**  
 581 **of the Cantabria University during the accumulation and ventilation phases of both instruments. Lower panel: Time**  
 582 **series of the radon fluxes obtained with the *AutoFlux* system (black dotted line), by the *INTE\_Flux* system (*Client*)**  
 583 **before the calibration factor being applied (red dotted line) and after its application (green dotted line).**

584  
 585  
 586

587

Table 4. Slope and Fluxes obtained by Eq. 10 for the *INTE\_Flux* system.

Slope $b$ ( $\text{Bq m}^{-3} \text{h}^{-1}$ )	$F_{Client}$ ( $\text{mBq m}^{-2} \text{s}^{-1}$ )
37239	1553
30325	1265
29629	1235
33301	1389
29209	1218
<b>Mean <math>\pm</math> Standard Deviation</b> <b>(1332 <math>\pm</math> 140) <math>\text{mBq m}^{-2} \text{s}^{-1}</math></b>	

588

589 To estimate the total uncertainty ( $u_{cal}$ ) of the calibration factor  $F_{Cal}$  in agreement with the ‘Guide to the Expression  
590 of Uncertainty in Measurement’ (JCGM 100) was used Eq. 19:

$$591 \left( \frac{u_{Cal}}{F_{Cal}} \right)^2 = \left( \frac{u_{Client}}{F_{Client}} \right)^2 + \left( \frac{u_{ref}}{F_{ref}} \right)^2 + \left( \frac{u_{Cal\_Autoflux}}{F_{Cal\_Autoflux}} \right)^2 \quad (19)$$

592 Thus, the calibration factor  $F_{Cal}$  value will be obtained with a total associated uncertainty equal to  $u_{Cal} = 0.12$  which  
593 corresponds to 9% of the calibration factor. To ensure a confidence level of 95% the Welch–Satterthwaite equation  
594 was used to calculate an approximation to the effective degrees of freedom of the  $u_{cal}$  variable and to select the  
595 corresponding t-student coverage factor. A total expanded uncertainty  $U_{cal} = 0.24$  ( $k=2$ ) was calculated.

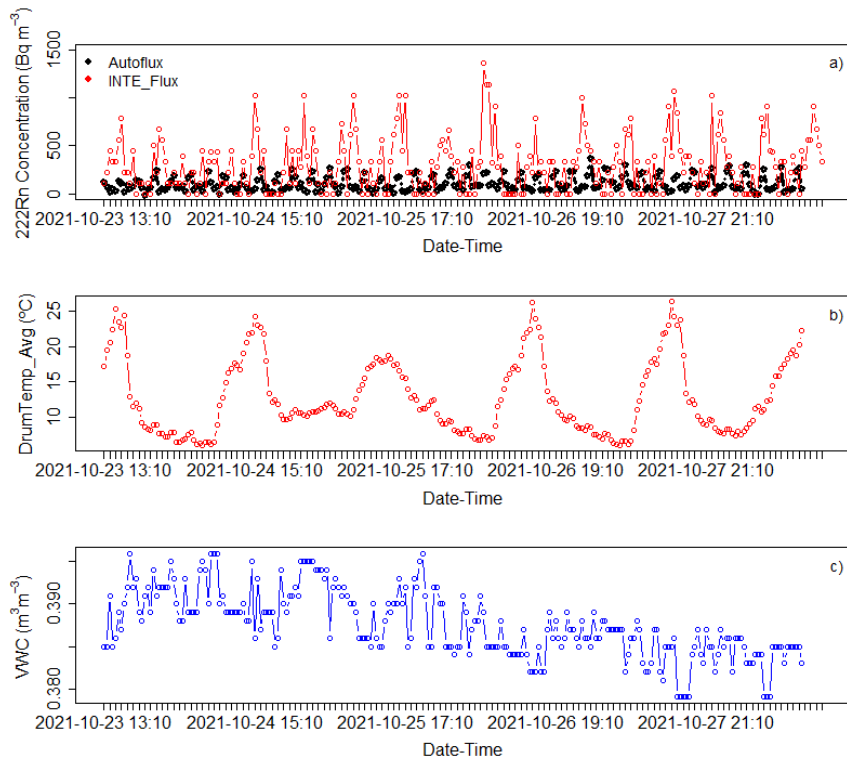
596

### 597 3.4 Short field comparison between TS, *INTE\_Flux* and modeled radon fluxes

598

599 The calibrated *Autoflux* and *INTE\_Flux* systems were used during two intercomparison campaigns presented by  
600 Rabago et al., 2022. Figure 7 shows time series of radon concentrations measured within both systems at a low  
601 radium content area campaign between the 23<sup>rd</sup> and the 28<sup>th</sup> of October, 2021 in Esles de Cayón, Spain (lat.: 43.28,  
602 long.: -3.80). Time series of measured VWC and drum temperature from the *Autoflux* are also shown. It can be  
603 noted that temperature cycles are mostly related with day/night atmospheric condition where the soil moisture  
604 shows a generally decreasing trend over the duration of the campaign. The reader should take into account that the  
605 higher radon concentrations measured by the *INTE\_Flux* system are inversely proportional to its smaller volume.

606



607  
608

609 **Figure 7. (a) Time series of radon concentrations measured by the *Autoflux*'s AG every 10 minutes (black dotted line)**  
 610 **and the *INTE\_Flux*'s DOSEman every 30 minutes (red dotted line), (b) drum temperature (red dotted line), and (c)**  
 611 **VWC (black dotted line) measured by *Autoflux* sensors.**

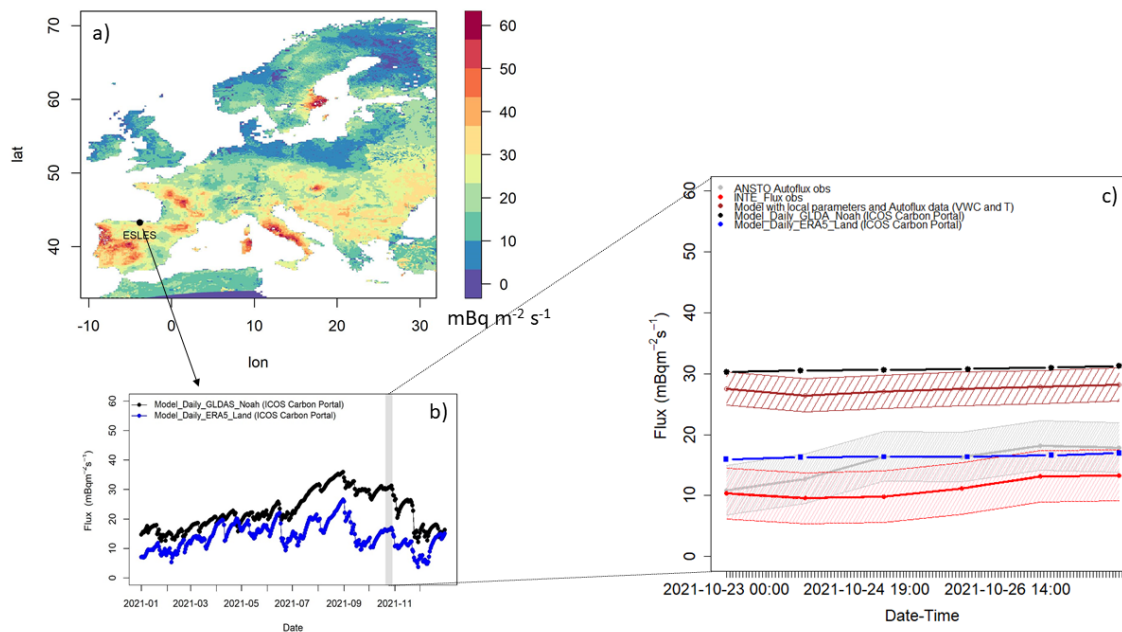
612 Daily mean radon fluxes measured by the *Autoflux* and *INTE\_Flux* systems throughout the campaign are shown  
 613 in Figure 8c together with:

- 614 i) Data from the traceRadon daily radon flux maps for Europe 2021 (Figure 8a) based on ERA5-Land  
 615 and on GLDAS-Noah v2.1 soil moisture reanalysis data (Figure 8b), respectively, available at the  
 616 ICOS Carbon Portal (Karstens, U. and Levin, I., 2022). Radon fluxes are calculated following  
 617 Karstens et al., 2015 and including the calculation of the emanation factor proposed by Zhuo et al.,  
 618 2008 but taking into account only half of the temperature influence ( $c/2$  in Eq. 12). The soil uranium  
 619 content and the soil properties needed to apply Eq. 1 within these maps were extracted by EANR,  
 620 2019 and ESDB, Hiederer, 2013, respectively.
- 621 ii) Radon fluxes calculated applying the model by Karstens et al., 2015 and the complete emanation  
 622 factor proposed by Zhuo et al., 2008 with soil temperature and soil moisture values measured by  
 623 *Autoflux* sensors during the measurement campaign. Uranium content of the soil and soil parameters  
 624 to apply Eq. 1 were directly measured in the laboratory on soil samples extracted at the measurement  
 625 site.

626

627 It can be observed that radon fluxes measured by the two calibrated systems are in agreement during the field  
 628 measurements and they increase throughout the campaign in accordance with the decrease in soil water content  
 629 (Figure 7c). Output of the model based on ERA5\_Land and GLDAS\_Noah data do not show any increase over the  
 630 measurement period.. Radon fluxes modeled using GLDAS\_Noah reanalysis data or local measured parameters  
 631 seem to be twice as high as experimental values and ERA5\_Land radon flux based data. This might be related to  
 632 a better estimation of the ERA5\_Land soil water content and to an underestimation of the soil water content  
 633 measured by the one-point sensor of the *Autoflux* and of the GLDAS\_Noah data for these days.

634



635  
 636 **Figure 8. a) Radon flux map for Europe for October 2021 based on GDAS\_Noah reanalysis data and Esles location; b)**  
 637 **Time series of daily radon fluxes for 2021 modeled using GLDAS\_Noah (black dots) and ERA5\_Land (Blue dots)**  
 638 **reanalysis data at Esles coordinates; c) Daily fluxes and standard deviations of: *Autoflux* observations (black dotted**  
 639 **line), *INTE\_Flux* observations (red dotted line), model based on measurements (brown dotted line), model based on**  
 640 **ERA5\_Land reanalysis (orange dotted line) and GLDAS\_Noah reanalysis (blue dotted line).**

641  
 642 **Conclusions**  
 643

644 Reliable long-term radon flux observations are important to validate radon flux maps used for radiation protection  
 645 and climate goals.

646 In the present study a new automatic radon flux system, which allows 3-hourly measurement of radon fluxes  
 647 together with environmental parameters in the soil and ambient air, has been characterized and calibrated for being  
 648 used as Transfer Standard to enable traceable radon flux measurements. This was done using a bespoke exhalation  
 649 bed built and characterized for this purpose. The new radon flux system (*Autoflux*) was then used to calibrate a  
 650 second radon flux monitor (*INTE\_Flux*). Both calibrated monitors were tested during a short in situ measurement  
 651 campaign and results were compared with ones obtained from available radon flux maps using soil properties  
 652 from European datasets (traceRadon daily radon flux maps for Europe 2021 based on ERA5-Land and on GLDAS-  
 653 Noah v2.1 soil moisture reanalysis data, respectively, available at the ICOS Carbon Portal) or local measurements.

654 The exhalation bed, designed and built as primary standard, was characterized both theoretically and  
 655 experimentally to check its reliability and to better understand how the variability of some soil conditions, such as  
 656 the water content, could influence the measured radon exhalation. The experimental approach allows a significant  
 657 reduction of the uncertainty of the radon exhalation rate.

658 Based on the results so far, the automatic *AutoFlux* system appears to be a reasonable option for a Transfer  
 659 Standard, however further studies of this kind should be carried out at lower reference radon exhalation rates (in  
 660 the order of tens  $\text{mBq m}^{-2} \text{s}^{-1}$ ) and under extreme environmental conditions of soil moisture and temperature to  
 661 better understand sub daily timescale variability of measured fluxes and to quantify the increase of the total flux  
 662 value uncertainty for these cases. In addition, the *AutoFlux* system, for low radon flux soils, may be used with a  
 663 continuous radon monitor with a faster response and an higher sensitivity in to allow to observe the linear increase  
 664 of the radon concentration within the accumulation chamber with the smallest possible standard deviation.

665 Daily radon flux observations during the short field intercomparison campaign carried out in northern Spain from  
 666 the two calibrated systems are coherent, within their daily standard deviations, and in agreement with the daily  
 667 radon fluxes modeled using ERA5\_Land reanalysis. Daily radon fluxes modeled using local measured parameters

668 and variable or GDAS\_Noah reanalysis data show higher values. This last result shows the importance to validate  
669 the input parameters (porosity, bulk density, etc.) and variable (i.e. volume water content and temperature in the  
670 soil) used within the model and to perform long-term measurements at different soils and under different  
671 meteorological conditions.

## 672 **Author Contributions**

673  
674 C. Grossi, D. Rabago, S. Chambers, R. Curcoll and A. Vargas led the data analysis and the writing of the  
675 manuscript. D. Rabago, C. Sáinz and L. Quindos carried out the literature study and the design, building and  
676 characterization of the Exhalation Bed facility. P.P.S. Otáhale and E. Fialová led the literature study of the radon  
677 flux systems. C. Grossi, A. Vargas and D. Rabago carried out the experimental and theoretical characterization of  
678 the *Autoflux* system. All authors participated in the discussion of the results and the writing of the manuscript.

679

## 680 **Acknowledgments**

681 Authors declare do not have any conflict of interest.

682 This study has been possible thanks to the project 19ENV01 traceRadon. The project 19ENV01 traceRadon has  
683 received funding from the EMPIR programme co-financed by the Participating States and from the European  
684 Union's Horizon 2020 research and innovation programme. 19ENV01 traceRadon denotes the EMPIR project  
685 reference.

686 Authors want to thank the work of Sylvester Werczynski, previously employed at ANSTO, who worked on the  
687 design and control software of the *Autoflux* system and of Ute Kartsens who made available the radon fluxes  
688 model data.

## 689 **Code and data availability**

690 The data and the codes from this study are available from the corresponding author and at the following link:  
691 [https://github.com/ClauGro/GRL\\_Data](https://github.com/ClauGro/GRL_Data). Scripts of the software R v. 3.6.2 (with Rstudio) and Python v. 3.8 (with  
692 Spyder) were used and are also shared in the github repository.

693

## 694 **References**

695

696 Altic, N. A. (2014). *Pilot study report for radon exhalation measurements*. Oak Ridge Associated  
697 Universities, Tennessee.

698

699 Baskaran, M. (2016). *Radon: A tracer for geological, geophysical and geochemical studies*. Springer. Detroit  
700 (USA). doi: 10.1007/978-3-319-21329-3.

701

702 Celaya González, S., Rábago Gómez, D., Fuente Merino, I., Quindós López, L., Bon Carreras, N., Valero  
703 Castell, M. T., Gutierrez Villanueva, J. L. & Sainz Fernández, C. (2018). A simple national intercomparison  
704 of radon in water. *Radiation Protection Dosimetry*, 181(4), 343-349.

705

706 Chambers, S.D. Williams, A.G. Conen, F. Griffiths, A.D. Reimann, S. Steinbacher, M. Krummel, P.B. Steele,  
707 L.P. van der Schoot, M.V. Galbally, I.E. Molloy, S.B. Barnes, J.E. (2015): Towards a universal “baseline”  
708 characterisation of air masses for high- and low-altitude observing stations using Radon-222, Aerosol and Air  
709 Quality Research 16, 885–899, doi: 10.4209/aaqr.2015.06.0391.

710

711 Chambers SD, Preunkert S, Weller R, Hong S-B, Humphries RS, Tositti L, Angot H, Legrand M, Williams  
712 AG, Griffiths AD, Crawford J, Simmons J, Choi TJ, Krummel PB, Molloy S, Loh Z, Galbally I, Wilson S,  
713 Magand O, Sprovieri F, Pirrone N and Dommergue A. (2018): Characterizing Atmospheric Transport  
714 Pathways to Antarctica and the Remote Southern Ocean Using Radon-222, *Front. Earth Sci.*, 6:190, doi:  
715 10.3389/feart.2018.00190.

716

717 Ferry C., Beneito A., Richon P. and Robe M.-C. (2001): An Automatic Device for Measuring the Effect of  
718 Meteorological Factors on Radon-222 Flux from Soils on the Long-term, *Radiation Protection Dosimetry*,  
719 Volume 93, Issue 3, 1 February 2001, Pages 271–274, doi: 10.1093/oxfordjournals.rpd.a006439.  
720

721 Grossi C., Vargas A., Camacho A., Lopez C. I., Bolívar J., Xia Y. and Conen F. (2011): Inter-Comparison of  
722 Different Direct and Indirect Methods to Determine Radon Flux from Soil. *Radiation Measurements*. 46. 112-  
723 118, doi: 10.1016/J.Radmeas.2010.07.021.  
724

725 Grossi, C., Vogel, F. R., Curcoll, R., Àgueda, A., Vargas, A., Rodó, X., and Morguá, J.-A. (2018): Study of  
726 the daily and seasonal atmospheric CH<sub>4</sub> mixing ratio variability in a rural Spanish region using <sup>222</sup>Rn tracer,  
727 *Atmos. Chem. Phys.*, 18, 5847–5860, doi: 10.5194/acp-18-5847-2018.  
728

729 Gutiérrez-Álvarez, I., Martín, J. E., Adame, J. A., Grossi, C., Vargas, A., & Bolívar, J. P. (2020a).  
730 Applicability of the closed-circuit accumulation chamber technique to measure radon surface exhalation rate  
731 under laboratory conditions. *Radiation Measurements*, 133, 106284, doi: 10.1016/j.radmeas.2020.106284.  
732

733 Gutiérrez-Álvarez, I., Guerrero, J. L., Martín, J. E., Adame, J. A., & Bolívar, J. P. (2020b). Influence of the  
734 accumulation chamber insertion depth to measure surface radon exhalation rates. *Journal of hazardous*  
735 *materials*, 393, 122344, doi: 10.1016/j.jhazmat.2020.122344.  
736

737 Hassan, N. M., Hosoda, M., Ishikawa, T., Sorimachi, A., Sahoo, S. K., Tokonami, S., and Fukushima, M. (2009).  
738 Radon migration process and its influence factors; review. *Japanese Journal of Health Physics*, 44(2), 218-  
739 231, doi: 10.5453/jhps.44.218.  
740

741 Hosoda, M., Shimo, M., Sugino, M., Furukawa, M., & Fukushima, M. (2007). Effect of soil moisture content  
742 on radon and thoron exhalation. *Journal of nuclear science and technology*, 44(4), 664-672, doi:  
743 10.1080/18811248.2007.9711855.

744 IAEA (2004). *Soil Sampling for Environmental Contaminants*, IAEA-TECDOC-1415, IAEA, Vienna.

745 IAEA (2013). *Measurement and Calculation of Radon Releases from NORM Residues*, IAEA-TECDOC-77,  
746 IAEA, Vienna.

747 Indoria, A. K., Sharma, K. L., & Reddy, K. S. (2020). Hydraulic properties of soil under warming climate.  
748 *Climate Change and Soil Interactions*, 473-508, doi: 10.1016/B978-0-12-818032-7.00018-7.  
749

750 ISO (2009). ISO 61577-7:2009. Equipment for the production of reference atmospheres containing radon  
751 isotopes and their decay products (STAR). ISO: Geneva, Switzerland.  
752

753 ISO/IEC (2015) 13528:2015. Statistical methods for use in proficiency testing by interlaboratory comparison.  
754 Jin, Y. and Jury, W. A. (1996): Characterizing the Dependence of Gas Diffusion Coefficient on Soil  
755 Properties, *Soil Sci. Soc. Am. J.*, 60, 66–71, doi: 10.2136/sssaj1996.0361599500600010012x.  
756

757 Karstens, U., Schwingshackl, C., Schmithüsen, D., and Levin, I. (2015): A process-based <sup>222</sup>radon flux map  
758 for Europe and its comparison to long-term observations, *Atmos. Chem. Phys.*, 15, 12845–12865, doi:  
759 10.5194/acp-15-12845-2015.  
760

761 Karstens, U. and Levin, I., 2022. traceRadon daily radon flux map for Europe 2021 (based on ERA5-Land  
762 soil moisture), <https://hdl.handle.net/11676/NvC7D-BVXlnHtFbDUSKpNVHT>, Access Date: 22<sup>nd</sup> August,  
763 2022.  
764

765 Karstens, U. and Levin, I., 2022<sup>b</sup>. traceRadon daily radon flux map for Europe 2021 (based on GLDAS-  
766 Noah v2.1 soil moisture), <https://hdl.handle.net/11676/JoDR653JxQuqLvEwzqI2kdMw>, Access Date: 22<sup>nd</sup>  
767 August, 2022.  
768

769 Levin, I., Karstens, U., Hammer, S., DellaColetta, J., Maier, F., and Gachkivskyi, M. (2021): Limitations of  
770 the radon tracer method (RTM) to estimate regional greenhouse gas (GHG) emissions – a case study for  
771 methane in Heidelberg, *Atmos. Chem. Phys.*, 21, 17907–17926, doi:[10.5194/acp-21-17907-2021](https://doi.org/10.5194/acp-21-17907-2021).  
772

773

774

775 López-Coto, J., Mas, J. L., and Bolivar, J. P. (2013). A 40- year retrospective European radon flux inventory  
776 including climatological variability, *Atmos. Environ.*, 73, 22–33, doi: 10.1016/j.atmosenv.2013.02.043.  
777

778 López-Coto I., Mas J. L., Bolivar J. P., García-Tenorio A. (2009): A short-time method to measure the radon  
779 potential of porous materials. *Applied Radiation and Isotopes* 67, 133–138, doi:  
780 10.1016/j.apradiso.2008.07.015.

781 McLaughlin T. (2011): Technical Bases And Guidance For Radon Flux Monitoring At Uranium Mill Tailing  
782 Sites. DOE CONTRACT NO. DE-AC05-06OR23100, (RFTA 11-010) DCN 2042-TR-01-0  
783

784 Millington, R. J. and Quirk, J. P. (1960). Transport in Porous media, Proceedings of the 7th International  
785 Congress of soil Science, Madison, Wisconsin, USA, 97–106.  
786

787 Morawska, L., 1989. Two ways of  $^{222}\text{Rn}$  determining the emanation coefficient. *Health Phys.* 57, 481-483,  
788 ISSN: 00179078.  
789

790 Nazaroff, W. W. (1992). Radon transport from soil to air. *Reviews of geophysics*, 30(2), 137-160, doi:  
791 doi.org/10.1029/92RG00055.  
792

793 Onishchenko, A., Zhukovsky, M., & Batrikov, V. (2015). Calibration system for measuring the radon flux  
794 density. *Radiation protection dosimetry*, 164(4), 582-586, doi: 10.1093/rpd/ncv315.

795 Porstendörfer, J. (1994). Properties and behaviour of radon and thoron and their decay products in the air.  
796 *Journal of Aerosol Science*, 25(2), 219-263, doi: 10.1016/0021-8502(94)90077-9.  
797

798 Prasad, G., Ishikawa, T., Hosoda, M., Sorimachi, A., Janik, M., Sahoo, S. K., ... & Uchida, S. (2012).  
799 Estimation of radon diffusion coefficients in soil using an updated experimental system. *Review of*  
800 *Scientific Instruments*, 83(9), 093503, doi: 10.1063/1.4752221.

801 Quindos, L. S., Fernandez, P. L., & Soto, J. (1994). A method for the measurement of the emanation factor  
802 for  $^{222}\text{Rn}$  in small samples of porous materials. *Radiation Protection Dosimetry*, 56(1-4), 171-173, ISSN 0144-  
803 8420.  
804

805 Rábago, D. Quindós, L. Vargas, Sainz, C. Radulescu, I. Ioan, I. Cardellini, F. Capogni, M. Celaya, S. Fuente,  
806 M. Grossi, C. (2022). Intercomparison of Radon Flux Monitors at Low and at High Radium Content Areas  
807 under Field Conditions. *International Journal of Environmental Research and Public Health*, 19(7), 4213. doi:  
808 10.3390/ijerph19074213.  
809

810 Rogers, V. C., & Nielson, K. K. (1991). Multiphase radon generation and transport in porous materials.  
811 *Health Physics*, 60(6), 807-815, doi: 10.1097/00004032-199106000-00006.

812 Röttger, S. Röttger, A. Grossi, C. Vargas, A. Karstens, U. Cinelli, G. Chung, E. Kikaj, D. Rennick, C. Mertes,  
813 F. Radulescu I. (2022): Radon metrology for use in climate change observation and radiation protection at the  
814 environmental level. *Advances in Geosciences*, 57, pp. 37–47, doi: 10.5194/adgeo-57-37-2022.  
815

816 Röttger, A. Röttger, S. Grossi, S. Vargas A. et al. (2021): New metrology for radon at the environmental level,  
817 *Measurement Science and Technology*, 32(12), 124008, doi: 10.1088/1361-6501/ac298d.  
818

819 Schery, S. D. and Wasiolek, M. A. (1998). Radon and Thoron in the Human Environment, chap. Modeling  
820 Radon Flux from the Earth's Surface, World Scientific Publishing, Singapore, 207–217.  
821

822 Schüßler, W. (1996). Effektive Parameter zur Bestimmung des Gasaustauschs zwischen Boden und  
823 Atmosphäre, PhD thesis, Heidelberg University, Germany.  
824

825 Stefani, N. Likos, W. J. Asce, M. Benson, C. (2016). Evaluation of Two Methods for Measuring Radon Flux  
826 from Earthen Radon Barriers. *Geo-Chicago 2016 GSP* 273, 145-155, WoS Id:000389439100016  
827

828 Stieff, L., Kotrappa, P., & Bigu, J. (1996). Passive E-perm radon flux monitors for measuring undisturbed  
829 radon flux from the ground. In *Proc. International Radon Symposium*, American Assoc. of Radon Scientists  
830 and Technologists, Haines City, FL.

831  
832 Stoulos, S., Manolopoulou, M., Papastefanou, C. (2004). Measurement of radon emanation factor from  
833 granular samples: effects of additives in cement. *Applied Radiation and Isotopes*, 60(1), 49-54, doi:  
834 10.1016/j.apradiso.2003.10.004.  
835  
836 Szegvary, T., Conen, F., Ciais, P. (2009): European <sup>222</sup>Rn inventory for applied atmospheric studies, *Atmos.*  
837 *Environ.*, 43, 1536–1539, doi: 10.1016/j.atmosenv.2008.11.025.  
838  
839 Tan, Y., & Xiao, D. (2011). Revision for measuring the radon exhalation rate from the medium surface. *IEEE*  
840 *Transactions on Nuclear Science*, 58(1), 209-213, doi: 10.1109/TNS.2010.2090897.  
841  
842 Tan, Y., & Xiao, D. (2013). A novel method to measure the radon exhalation rate in only one measurement  
843 cycle. *Analytical Methods*, 5(3), 805-808, doi: 10.1039/C2AY26134K.  
844  
845 Tan, Y., Yuan, H., Xie, Y., Liu, C., Liu, X., Fan, Z., & Kearfott, K. (2020). No flow meter method for  
846 measuring radon exhalation from the medium surface with a ventilation chamber. *Applied Radiation and*  
847 *Isotopes*, 166, 109328, doi: 10.1016/j.apradiso.2020.109328.  
848  
849 UNSCEAR. United Nations Scientific Committee on the Effects of Atomic Radiation. (1988). *Sources, effects*  
850 *and risks of ionizing radiation*. New York. ISBN 92-1- 142143-8.  
851  
852 Yang J., Buchsteiner M., Salvamoser J., Irlinger J., Guo Q. And Tschiersch J. (2017) Radon Exhalation From  
853 Soil And Its Dependence From Environmental Parameters, *Radiation Protection Dosimetry* 177,1-2, 21–25,  
854 doi:10.1093/Rpd/Ncx165.  
855  
856 Zahorowski, W. and Whittlestone, S. (1996). A fast portable emanometer for field measurements of radon  
857 and thoron flux. *Radiation Protection Dosimetry*, 67, 2, 109-120, doi: 10.1093/oxfordjournals.rpd.a031802.  
858  
859 Zhang, B. Liu, H. Crawford, J.H. Chen ,G. Fairlie, T.D. Chambers, S.D. Kang, C.-H. Williams, A.G. Zhang,  
860 K. Considine, D.B. Sulprizio, M.P. Yantosca, R.M. (2021): Simulation of radon-222 with the GEOS-Chem  
861 global model: Emissions, seasonality, and convective transport, *Atmospheric Chemistry and Physics* 21,  
862 1861-1887, doi:10.5194/acp-21-1861-2021.  
863  
864 Zhuo, W., Iida, T., and Furukawa, M. (2006): Modeling radon flux density from the Earth's surface, *J. Nucl.*  
865 *Sci. Technol.*, ISSN 0022-3131, 43(4), 479-482.  
866  
867 Zhuo, W., Guo, O., Chen, B., and Cheng, G. (2008): Estimating the amount and distribution of radon flux  
868 density from the soil surface in China, *J. Environ. Radioactiv.*, 99, 1143–1148, doi:  
869 10.1016/j.jenvrad.2008.01.011.  
870  
871